Fine structures of azimuthal correlations of two gluons in the glasma

Hengying Zhang,[1] Donghai Zhang,[1] Yeyin Zhao,[1] Mingmei Xu,[1,*] Xue Pan,[2] and Yuanfang Wu[1,†]

[1]*Key Laboratory of Quark and Lepton Physics (MOE) and Institute of Particle Physics, Central China Normal University, Wuhan 430079, China*

[2]*School of Electronic Engineering, Chengdu Technological University, Chengdu 611730, China*

(Received 13 October 2017; published 5 February 2018)

We investigate the azimuthal correlations of the glasma in p-p collisions at $\sqrt{s_{\mathrm{NN}}} = 7$ TeV by using the color glass condensate (CGC) formalism. As expected, the azimuthal correlations show two peaks at $\Delta\phi = 0$ and π, which represent collimation production in the CGC. Beyond that, azimuthal correlations show fine structures, i.e., bumps or shoulders between the two peaks, when at least one gluon has small x. The structures are demonstrated to be associated with saturation momentum and likely appear at transverse momentum around $2Q_{\mathrm{sp}} = 1.8$ GeV/c.

DOI: 10.1103/PhysRevD.97.034003

I. INTRODUCTION

Two-particle correlations in high-energy collisions have been measured previously for a broad range of collision energies and colliding systems with the goal of understanding the underlying mechanism of particle production. Especially, the study of two-particle azimuthal correlations provides important information for characterizing QCD, e.g., the mechanism of hadronization, the possible collective effect, and the gluon saturation effect in these collisions.

One measurement of azimuthal correlations is performed using two-dimensional $\Delta\eta$-$\Delta\phi$ correlation functions. Here, $\Delta\eta$ is the difference in pseudorapidity between the two particles, and $\Delta\phi$ is the difference in their azimuthal angle (in radians). Another measurement of azimuthal correlations is projection of two-dimensional (2D) correlation functions onto $\Delta\phi$, i.e., $\Delta\phi$ distributions, usually at short-range rapidity (small $\Delta\eta$) and long-range rapidity (large $\Delta\eta$).

In minimum-bias p-p collisions, both in the data and in the Monte Carlo event generator PYTHIA, the two-dimensional $\Delta\eta$-$\Delta\phi$ correlations in the intermediate $p_\perp$ range are dominated by two components [1–3]: a narrow peak at $(\Delta\eta, \Delta\phi) \approx (0, 0)$, which can be understood as the contribution from jets, and a ridge at $\Delta\phi \approx \pi$ extending over a broad range in $\Delta\eta$, interpreted as due to momentum conservation or away-side jets. If this azimuthal correlations are demonstrated as $\Delta\phi$ distribution at long-range rapidity ($|\Delta\eta| > 2$), there is a peak at the away side ($\Delta\phi \approx \pi$) and no peak at the near side ($\Delta\phi \approx 0$) in minimum-bias p-p collisions. However, in central heavy-ion collisions, e.g., Au-Au [1,2,4,5] and Pb-Pb [6] collisions, the azimuthal correlations measured in the intermediate $p_\perp$ range begin to show an elongated structure in the $\Delta\eta$ direction at the near side, known as the near-side ridge. The corresponding $\Delta\phi$ distribution at large $\Delta\eta$ starts to show a peak at the near side that is absent in minimum-bias p-p collisions.

Later, high-multiplicity events in small systems, like p-p and p-Pb collisions at the LHC [3,6–10] and d-Au and He-Au collisions at the Relativistic Heavy Ion Collider [11,12] also show a near-side ridge phenomenon that is similar to that of the heavy-ion collisions. Careful subtraction of the azimuthal correlations in low-multiplicity events from those in high-multiplicity events shows that the magnitude of the near-side peak is nearly identical to that of the away-side peak, known as the double-ridge phenomenon [8–10]. Collimated production in the azimuthal angle is a prominent feature at long-range rapidity.

Azimuthal correlations at long-range rapidity in small systems can be explained by initial-state effects such as gluon saturations [13–17], final-state parton-parton induced interactions [18], hydrodynamic flow [19–21], etc. Among these explanations, the use of the hydrodynamic model for small systems such as p-p and p-A collisions is still under intense debate due to the doubt about fast thermalization. On the other hand, without flow, the dihadron azimuthal correlations at long-range rapidity calculated from a combination of glasma dynamics and Balitsky-Fadin-Kuraev-Lipatov evolution (dominating the away-side peak) agree well with data in p-p and p-Pb collisions over a very wide range of $p_\perp^{\mathrm{trig}}$, $p_\perp^{\mathrm{asc}}$ windows, centrality classes, and $\Delta\eta$ acceptance on a quantitative level [15–17]. The agreement

*xumm@mail.ccnu.edu.cn
†wuyf@phy.ccnu.edu.cn

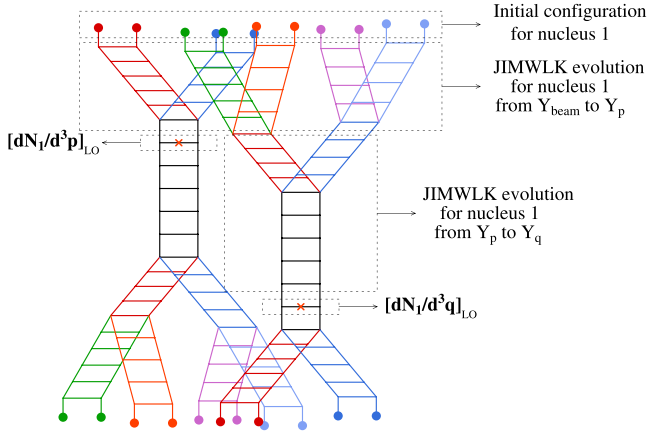

FIG. 1. A schematic diagram of high-energy QCD evolution. Two crosses mark two observed gluons with momentum $\mathbf{p}$ and $\mathbf{q}$. Y_p and Y_q denote their rapidities in the infinite momentum frame, i.e., $Y = \ln\frac{x_0}{x}$. The lower part of the figure, representing nucleus 2, is made up of identical evolution. The figure is reprinted from Ref. [14], copyright 2010, with permission from Elsevier.

suggests that gluon saturation in the initial state is the most promising explanation and two-particle azimuthal correlations are sensitive to detailed dynamical features of the color glass condensate (CGC).

In the glasma picture, the boost invariance of color flux tubes in high-energy collisions plays an important role in understanding the long-range rapidity correlations [13]. Under that picture, the roles of the various x degrees of freedom of gluons (i.e., Feynman x, the longitudinal momentum fraction in the projectile or target) were studied carefully in our previous paper [22]. Gluons are progressively emitted from valence quarks by the ladder graph, shown in Fig. 1. The smaller the x of a gluon, the later the gluon evolves. Furthermore, the mechanism of gluon production in the various regions of phase space are different. For a right-moving parton, its rapidity y and transverse momentum $p_\perp$ are related to its Feynman x as $x = \frac{m_\perp}{\sqrt{s}}e^y$ in the high-energy limit. At $\sqrt{s} = 7$ TeV and intermediate $p_\perp$, e.g., 2 GeV/c, the rapidity at $y = 1$ corresponds to $x \sim 10^{-3}$, while $y = 2$ corresponds to $x \sim 10^{-2}$. This means that the gluon at the central rapidity region reflects the properties of the small-x ($x < 10^{-3}$) degrees of freedom, where the quantum evolutions are essential. In contrast, the gluon at the middle rapidity region presents the features of moderate-x ($10^{-3} < x < 10^{-2}$) degrees of freedom, where the quantum effects become weak, and the contributions of color sources have to be taken into account. The large-x ($x > 10^{-2}$) degrees of freedom act as sources of the small-x degrees of freedom. The evolution toward small x induces correlations with the color sources. The gluonic color sources are correlated over long distances to ensure the color neutrality. So, the ridge indicates the stronger correlation between the gluon of the color source and radiated gluon.

The azimuthal angle together with transverse momentum and rapidity constitute the 3-momentum of a particle. The distributions and correlations of the azimuthal angle are necessarily influenced by transverse momentum and rapidity due to, e.g., momentum conservation. Besides, for the study of the rapidity and transverse momentum dependence of azimuthal correlations, the CGC is unique for the following reasons:

(1) In the CGC, the mechanisms of gluon production in the various regions of phase space are different. Gluons at the central rapidity region reflect the properties of the small-x ($x < 10^{-3}$) degrees of freedom, and gluons with larger rapidity have larger x in the right-moving projectile. Since long-range ridgelike rapidity correlation can be explained by the stronger correlation between the gluon of the color source and radiated gluon, it is interesting to see how the x degrees of freedom affect the azimuthal correlations. Since gluons at different rapidity locations have different x, it is highly worth studying the rapidity location dependence of the azimuthal correlations.

(2) In the CGC, the transverse momentum distribution of saturated gluons (called uGD) has a peak, the position of which is called the characteristic transverse momentum of gluons and equals the saturation scale Q_s. That means uGD only takes a large value when $p_\perp$ is around Q_s. Since uGD determines the correlation function (as to be illustrated in Sec. II), the azimuthal correlations should be $p_\perp$ dependent and sensitive. Especially, $p_\perp$ also relates to Feynman x, and finer binning in $p_\perp$ helps to explore the contributions of different x degrees of freedom.

A systematic study of azimuthal anisotropy and its $p_\perp$ and y dependence is important because the regions of phase space are related to different x degrees of freedom. And, hence, it may supply special signals originating from CGC dynamics. It could provide crucial tests as to whether an initial-state interaction or a final-state interaction dominates the azimuthal correlation created in small systems. In this paper, we analyze the azimuthal correlations of p-p collisions at 7 TeV under the CGC framework. Most of the existing results in the references are limited by the range of the rapidity gap, such as long-range rapidity ($|\Delta\eta| > 2$) or short-range rapidity ($|\Delta\eta| < 1$), no matter in which rapidity location the gluons are situated. However, the analysis in this paper is not limited by the range of the rapidity gap but by the rapidity location, i.e., small rapidity region (defined as $|y| \leq 1$) and large rapidity region ($|y| \geq 2$).

This paper is organized as follows. In Sec. II, the definition of azimuthal correlation and some related formula of the single- and double-gluon inclusive production in the CGC framework are given. The formulas in this manuscript follow those in Refs. [13–17] and are identical to those at the gluon level, without fragmentation functions. The new aspects of analysis method here lie in the exploration of the

contributions of different x degrees of freedom, which are twofold: (i) the study on the effect of the longitudinal rapidity location on the azimuthal correlations and (ii) finer binning in $p_\perp$. Results of two-gluon azimuthal correlations are shown and discussed in Sec. III, in which the sensitivity to the rapidity location and transverse momentum are carefully compared and some interesting correlation patterns are illustrated. Section IV gives the summary and discussion.

II. TWO-GLUON AZIMUTHAL CORRELATIONS FROM HIGH-ENERGY QCD EVOLUTION

In a high-energy collision, both the projectile and the target are regarded as high parton density sources. When they pass through each other, strong longitudinal color electric and color magnetic fields are formed. The collection of the primordial fields at the early stage is called the glasma. The framework to describe the physics of high parton densities and gluon saturation is the CGC effective field theory [23–26]. The effective degrees of freedom in this framework are color sources ρ at large x and classical gauge fields $\mathcal{A}_\mu$ at small x. The classical gauge field $\mathcal{A}_\mu$ is the solution of Yang-Mills equations with a fixed configuration of color sources. For a given initial configuration of the color source, the distribution of sources and fields in the nuclear wave functions evolve with rapidity Y or corresponding x, which is described by the Jalilian-Marian-Iancu-McLerran-Weigert-Kovner (JIMWLK) renormalization group equations [27–29], as shown in Fig. 1. Here, Y can be translated to the rapidity of a gluon in the center-of-mass frame y, i.e., $Y = \ln\frac{x_0}{x} = \ln x_0 + \ln\frac{\sqrt{s}}{m_\perp} \pm y$. In Fig. 1, the dots at the upper part represent the initial color sources for nucleus 1. The ladder graphs following it illustrate the high-energy evolution of parton distribution, from Y_{beam} to Y_p and from Y_p to Y_q by the JIMWLK equation, with both radiation and scattering processes included. Two crosses mark two observed gluons with momentum $\mathbf{p}$ and $\mathbf{q}$. At first glance, the two gluons seem to be uncorrelated since they come from superficially disconnected diagrams. However, the two-gluon production should be calculated by averaging over the initial distribution of color sources, which introduces correlations.

Supposing two gluons are produced with transverse momentum $\boldsymbol{p}_\perp$ and $\boldsymbol{q}_\perp$, and rapidity y_p and y_q, two-particle correlation is defined as

$$C(\boldsymbol{p}_\perp, y_p; \boldsymbol{q}_\perp, y_q) = \frac{\left\langle \frac{dN_2}{d^2\boldsymbol{p}_\perp dy_p d^2\boldsymbol{q}_\perp dy_q}\right\rangle}{\left\langle \frac{dN_1}{d^2\boldsymbol{p}_\perp dy_p}\right\rangle\left\langle \frac{dN_1}{d^2\boldsymbol{q}_\perp dy_q}\right\rangle} - 1 = \frac{\left\langle \frac{dN_2^{\text{corr}}}{d^2\boldsymbol{p}_\perp dy_p d^2\boldsymbol{q}_\perp dy_q}\right\rangle}{\left\langle \frac{dN_1}{d^2\boldsymbol{p}_\perp dy_p}\right\rangle\left\langle \frac{dN_1}{d^2\boldsymbol{q}_\perp dy_q}\right\rangle}, \quad (1)$$

where $\left\langle \frac{dN_2}{d^2\boldsymbol{p}_\perp dy_p d^2\boldsymbol{q}_\perp dy_q}\right\rangle$ and $\left\langle \frac{dN_1}{d^2\boldsymbol{p}_\perp dy_p}\right\rangle$ are the double- and single-gluon inclusive productions and $\left\langle \frac{dN_2^{\text{corr}}}{d^2\boldsymbol{p}_\perp dy_p d^2\boldsymbol{q}_\perp dy_q}\right\rangle$ is the correlated double-gluon production that subtracts the uncorrelated double-gluon production. The leading-log factorization formula reads [13]

$$\langle\mathcal{O}\rangle_{\text{LLog}} = \int [D\rho_1][D\rho_2] W[\rho_1] W[\rho_2] \mathcal{O}[\rho_1,\rho_2]_{\text{LO}}, \quad (2)$$

where $\mathcal{O}[\rho_1,\rho_2]_{\text{LO}}$ is the leading-order single- or double-particle inclusive distribution for a fixed distribution of color sources, and the integration denotes an average over different distributions of the color sources with the weight functional $W[\rho_{1,2}]$. In general, $W[\rho_{1,2}]$ encodes all possible color charge configurations of the projectile and target and obeys the JIMWLK renormalization group equations [27–29]. In a mean field approximation and the large-N_c limit, the JIMWLK equation is reduced to the Balitsky-Kovchegov (BK) equation [30–32].

The averaging over color sources can be done under the McLerran-Venugopalan (MV) model with a Gaussian weight functional. According to Ref. [14], the correlated two-gluon production can be expressed by uGD as

$$\left\langle \frac{dN_2^{\text{corr}}}{d^2\boldsymbol{p}_\perp dy_p d^2\boldsymbol{q}_\perp dy_q}\right\rangle = \frac{C_2}{\boldsymbol{p}_\perp^2\boldsymbol{q}_\perp^2}\int_0^\infty d^2\boldsymbol{k}_\perp (D_1 + D_2), \quad (3)$$

where $C_2 = \frac{\alpha_s^2 N_c^2 S_\perp}{4\pi^{10}(N_c^2-1)^3}$ and

$$D_1 = \Phi_A^2(y_p,\boldsymbol{k}_\perp)\Phi_B(y_p,\boldsymbol{p}_\perp - \boldsymbol{k}_\perp)D_B,$$
$$D_2 = \Phi_B^2(y_q,\boldsymbol{k}_\perp)\Phi_A(y_p,\boldsymbol{p}_\perp - \boldsymbol{k}_\perp)D_A, \quad (4)$$

with

$$D_{A(B)} = \Phi_{A(B)}(y_q,\boldsymbol{q}_\perp + \boldsymbol{k}_\perp) + \Phi_{A(B)}(y_q,\boldsymbol{q}_\perp - \boldsymbol{k}_\perp). \quad (5)$$

Here, $\Phi_{A(B)}(y,\boldsymbol{k}_\perp)$ denotes the uGD of projectile A or target B. The single-gluon inclusive production reads

$$\left\langle \frac{dN_1}{d^2\boldsymbol{p}_\perp dy_p}\right\rangle = \frac{\alpha_s N_c S_\perp}{\pi^4(N_c^2-1)}\frac{1}{\boldsymbol{p}_\perp^2}\int\frac{d^2\boldsymbol{k}_\perp}{(2\pi)^2}\Phi_A(y_p,\boldsymbol{k}_\perp)\Phi_B(y_p,\boldsymbol{p}_\perp - \boldsymbol{k}_\perp). \quad (6)$$

The framework is valid to leading-logarithmic accuracy in x and momentum $p_\perp$, $q_\perp \gg Q_s$, and we only calculate the leading contributions in $p_\perp/Q_s$.

The important ingredient in the above expressions is uGD (Φ), which can be obtained by solving the BK equation with running coupling corrections with a given initial condition. To avoid repetition, details can be found in Ref. [14] and our previous paper [22]. For p-p collision at 7 TeV, Q_{s0}^2 (with Q_{s0} the initial value of Q_s at x_0) is chosen to be 0.168 GeV^2 [15].

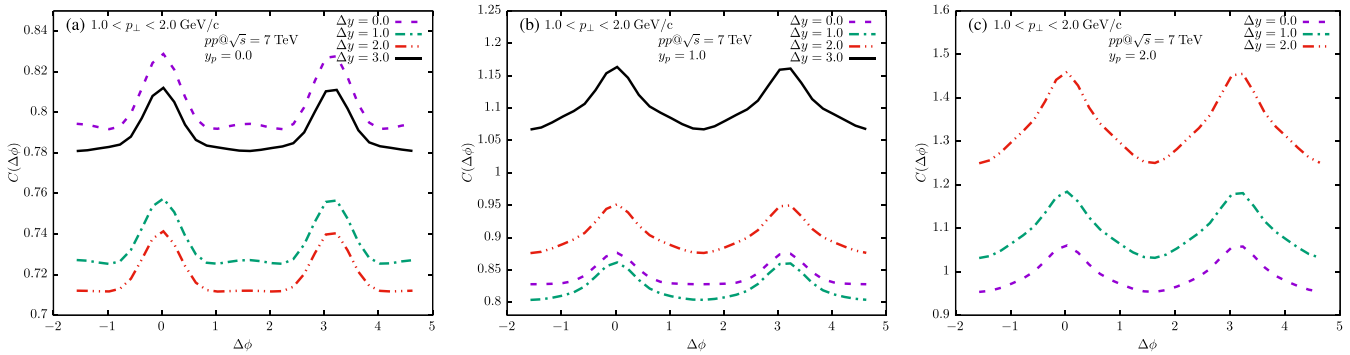

FIG. 2. The azimuthal correlation integrated in $1 < p_\perp < 2$ GeV/c and $1 < q_\perp < 2$ GeV/c is plotted as a function of $\Delta\phi$ for different rapidity gaps $\Delta y = y_q - y_p$ when one gluon is located at (a) $y_p = 0.0$, (b) $y_p = 1.0$, (c) $y_p = 2.0$, respectively.

Based on the correlation function $C(\boldsymbol{p}_\perp, y_p; \boldsymbol{q}_\perp, y_q)$, the azimuthal correlation function is defined as

$$C(\Delta\phi) = \int_{p_\perp^{\min}}^{p_\perp^{\max}} \frac{dp_\perp^2}{2} \int_{q_\perp^{\min}}^{q_\perp^{\max}} \frac{dq_\perp^2}{2} \times \int d\phi_p \int d\phi_q \delta(\phi_q - \phi_p - \Delta\phi) C(\boldsymbol{p}_\perp, y_p; \boldsymbol{q}_\perp, y_q), \tag{7}$$

which describes the correlation of two particles with rapidity y_p and y_q and their azimuthal separation $\Delta\phi$ in given transverse momentum intervals $(p_\perp^{\min}, p_\perp^{\max})$ and $(q_\perp^{\min}, q_\perp^{\max})$. We do not integrate over rapidity y because we focus on correlations between two gluons in given rapidity locations. The rapidity gap is defined as $\Delta y = y_q - y_p$.

III. FINE STRUCTURE OF AZIMUTHAL CORRELATION AND ITS TRANSVERSE MOMENTUM AND RAPIDITY DEPENDENCE

Both experimental data [3,10] and the CGC [15–17] show that the correlation at the near side gets strongest in an intermediate $p_\perp$ interval, approximately $1 < p_\perp < 3$ GeV/c. A calculation from the CGC points out that the correlation function gets a maximum at $p_\perp \sim Q_{sA} + Q_{sB} = 2Q_{sp} = 1.8$ GeV/c for minimum-bias p-p collisions, where $Q_{sA(B)}$ denotes the saturation momentum of the projectile or target [22]. To obtain the strongest correlation, the correlation function is first calculated within $1 < p_\perp < 2$ GeV/c in this paper.

To see how the azimuthal correlations change with rapidity gap and rapidity location, the azimuthal correlations are calculated at $\Delta y = 0$, 1, 2, 3 with the rapidity location of one gluon chosen to be $y_p = 0$, 1, 2 so that both the small rapidity location and large rapidity location are included. The results are shown in Fig. 2. As mentioned in Ref. [17], the azimuthal correlation from the CGC shows a symmetric structure about $\pi/2$; i.e., one peak is located at the near side $\Delta\phi = 0$, and the other peak is located at the away side $\Delta\phi = \pi$, which represents collimation production in the CGC. Here, we reproduce that structure in different rapidity locations, as all curves in Figs. 2(a), 2(b), and 2(c) show. Especially for long-range rapidity, e.g., $\Delta y = 2.0$ as red curves show, correlations show two peaks at $\Delta\phi = 0$ and π, which contributes to the double-ridge phenomenon observed in the data.

When one gluon is located at small rapidity, e.g., $y_p = 0.0$ shown in Fig. 2(a), the correlation strength at $\Delta\phi = 0$ decreases when the rapidity gap increases from 0 to 2 and then rises significantly when the rapidity gap gets 3, which reproduces the trend of rapidity correlation at $\Delta\phi = 0$ in Ref. [22] (Fig. 4 therein). The correlation strength at $\Delta y = 0$ is rather high, compared to that of $\Delta y = 1$ and 2, which is due to the contribution of short-range correlation at $\Delta y = 0$ from quantum evolution and is affected by the strength of the running coupling [33]. The correlation strength at $\Delta y = 3$ is rather high, which is long-range correlation in rapidity resulting from longitudinal boost invariance in the picture of color flux tubes of glasma [13]. The dependence of the correlation strength on the rapidity gap was discussed in detail in our previous papers [22,33] and is not the focus in this paper.

Besides the magnitude of correlations, the shape of the correlations as a function of $\Delta\phi$ shows interesting features. The two peaks at $\Delta\phi = 0$ and π exist in all cases in the following, and the focus of this paper is the correlation structure between the two peaks. In Fig. 2(a), the curve around $\Delta\phi = \pi/2$ shows a moderate bump at $\Delta y = 0$, which persists at $\Delta y = 1$ and flattens at $\Delta y = 2$ and finally turns into a shallow valley in the case of $\Delta y = 3$. In Fig. 2(b), the curve around $\Delta\phi = \pi/2$ shows a flat structure at $\Delta y = 0$, which reduces gradually to a valley at $\Delta y = 1$, 2, and 3. In Fig. 2(c), all curves show a valley around $\Delta\phi = \pi/2$, no matter if it is at short-range rapidity ($\Delta y = 0$, 1) or long-range rapidity ($\Delta y = 2$). Comparing the three subfigures for different rapidity locations, the bump around $\Delta\phi = \pi/2$ is limited to the small rapidity location.

Specifically, for azimuthal correlations at short-range rapidity $\Delta y = 0$, as can be seen from the purple curves in

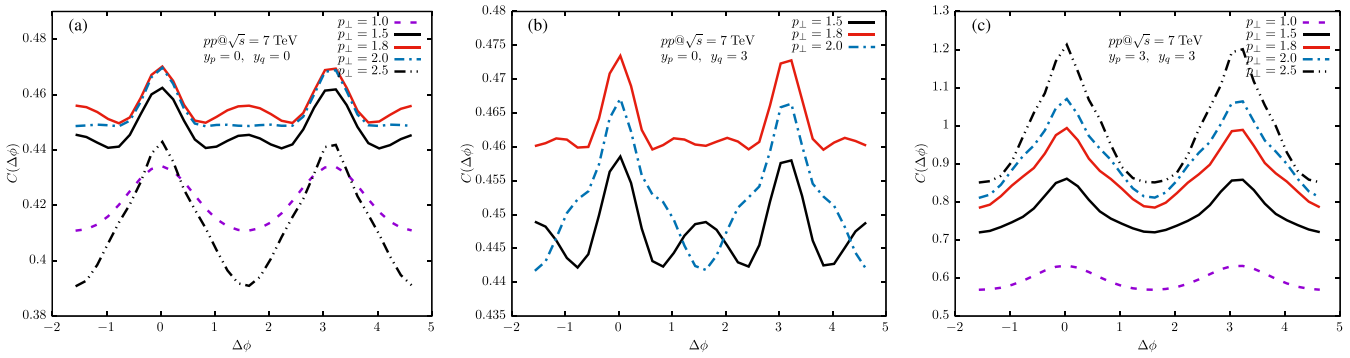

FIG. 3. Azimuthal correlation at five values of $p_\perp$ with $p_\perp = q_\perp$ at (a) $y_p = 0$, $y_q = 0$; (b) $y_p = 0$, $y_q = 3$; and (c) $y_p = 3$, $y_q = 3$. In (b), the curves for $p_\perp = 1.0$ and 2.5 GeV/c are similar to those in (a) and not shown in order to make the fine structure of other curves visible.

Figs. 2(a), 2(b), and 2(c), a bump appears at $\Delta\phi = \pi/2$ when $y_p = 0$, and it disappears at $y_p = 1$ and 2, which indicates that azimuthal correlations at short-range rapidity vary with the rapidity location of the chosen gluon. The azimuthal correlations at long-range rapidity also vary according to the rapidity location of the chosen gluon, as can be seen from the red curves in Figs. 2(a), 2(b), and 2(c). It suggests that azimuthal correlations at the same rapidity gap change with the rapidity location of the chosen gluon.

To obtain the azimuthal correlations at different rapidity locations in detail, we calculate the correlations between two gluons both at small rapidity, e.g., $y_p = 0$, $y_q = 0$ shown in Fig. 3(a); two gluons both at large rapidity, e.g., $y_p = 3$, $y_q = 3$ shown in Fig. 3(c); and one gluon at small rapidity and the other at large rapidity, e.g., $y_p = 0$, $y_q = 3$ shown in Fig. 3(b). Since azimuthal correlations are $p_\perp$ sensitive, an integration over $p_\perp$ may smear some correlation structure. Five values of $p_\perp$ are tried in the following calculations, i.e., $p_\perp = 1.0$, 1.5, 1.8, 2.0, 2.5 GeV/c. For simplicity, $q_\perp$ is chosen to be equal to $p_\perp$ at first.

Correlation patterns are more diverse at single $p_\perp$. In Fig. 3(a), the correlation at $p_\perp = 1.0$ GeV/c shows a valley at $\Delta\phi = \pi/2$. As $p_\perp$ increases to 1.5 GeV/c, a moderate bump at $\Delta\phi = \pi/2$ begins to appear and strengthens at $p_\perp = 1.8$ GeV/c. As $p_\perp$ increases further to 2.0 GeV/c, the correlation at $\Delta\phi = \pi/2$ drops to a flat structure and finally returns to a valley at a larger $p_\perp$ of 2.5 GeV/c. In Fig. 3(b), the curves for $p_\perp = 1.0$ and 2.5 GeV/c are similar to those in (a) and are hence not shown in order to make the fine structures of other curves visible. The correlation patterns at $p_\perp = 1.5$ GeV/c are similar to those in Fig. 3(a), while for $p_\perp = 1.8$ GeV/c, two bumps appear on the two sides of $\Delta\phi = \pi/2$, approximately at $\Delta\phi \approx 1.0$ and $\Delta\phi \approx 2.0$. Compared with the flat structure of $p_\perp = 2.0$ GeV/c in Fig. 3(a), a valley appears in Fig. 3(b), with two shoulders on the two sides of $\Delta\phi = \pi/2$. It is worth noticing that the positions of the two shoulders are almost the same as those of the two bumps of $p_\perp = 1.8$ GeV/c. However, all the bumps and flat structure existing in Figs. 3(a) and 3(b), which we call fine structures in the following, nearly disappear in Fig. 3(c), with only slight shoulders on the two sides of $\Delta\phi = \pi/2$ at $p_\perp = 1.8$ GeV/c and 2.0 GeV/c.

The above-mentioned phenomenon that azimuthal correlations at the same rapidity gap change with the rapidity location of the chosen gluon is more obvious in Figs. 3(a) and 3(c), in which the rapidity gap is the same, i.e., $\Delta y = 0$. By comparing the red curves in Figs. 3(a) and 3(c), we can see that the bump at $\Delta\phi = \pi/2$ only exists in the small rapidity location. Furthermore, the bumps (one or two) around $\Delta\phi = \pi/2$ only exist in Figs. 3(a) and 3(b), which further indicates that these fine structures require at least one gluon located at small rapidity. Not only that, but correlations calculated at single $p_\perp$ rather than integration in a wide $p_\perp$ range help to obtain these patterns. Single $p_\perp$ at 1.5, 1.8, and 2.0 GeV/c, i.e., a value near $p_\perp \sim 2Q_{\rm sp} = 1.8$ GeV/c, are most likely to show fine structures between $\Delta\phi = 0$ and π. This means that azimuthal correlations have a sensitive range in transverse momentum, a rough interval between 1.5 and 2.0 GeV/c, which is associated with the saturation momentum of colliding particles.

In fact, the single bump at $\Delta\phi = \pi/2$ and the double bumps or shoulders at $\Delta\phi \approx 1.0$ and $\Delta\phi \approx 2.0$ represent two harmonic components in the azimuthal correlations. The single bump at $\Delta\phi = \pi/2$ represents a component of $\cos(4\Delta\phi)$ with its local maximum at $\Delta\phi = \pi/2$. The double bumps or shoulders represent a component of $\cos(6\Delta\phi)$ with its local maximum at $\Delta\phi = \pi/3 \approx 1.0$ and $\Delta\phi = 2\pi/3 \approx 2.0$. The difference between double bumps and double shoulders lies in the large and small values of the coefficients of the sixth-order harmonic component. In the same way, the main peaks at $\Delta\phi = 0$ and $\Delta\phi = \pi$ represent a dominant component of $\cos(2\Delta\phi)$. If a Fourier expansion is applied to the azimuthal correlation function $C(\Delta\phi)$, it is natural to get the second-order, fourth-order, and sixth-order harmonic coefficients. High-order harmonic components only get prominent when at least one gluon is located at small rapidity and has transverse momentum near two times the saturation momentum of the colliding proton, i.e., $2Q_{\rm sp} = 1.8$ GeV/c.

The explanation of the patterns in azimuthal correlations depends on mechanism in this calculation. By the glasma graph shown in Fig. 1, the correlation function is proportional to the correlated two-gluon production and can be expressed by a convolution of four uGDs as shown in Eqs. (3), (4), and (5). The integrand of Eq. (3) is explicitly written as

$$D_1 = \Phi_A^2(y_p,\boldsymbol{k}_\perp)\Phi_B(y_p,\boldsymbol{p}_\perp-\boldsymbol{k}_\perp)\Phi_B(y_q,\boldsymbol{q}_\perp+\boldsymbol{k}_\perp) + \Phi_A^2(y_p,\boldsymbol{k}_\perp)\Phi_B(y_p,\boldsymbol{p}_\perp-\boldsymbol{k}_\perp)\Phi_B(y_q,\boldsymbol{q}_\perp-\boldsymbol{k}_\perp); \quad (8)$$

$$D_2 = \Phi_B^2(y_q,\boldsymbol{k}_\perp)\Phi_A(y_p,\boldsymbol{p}_\perp-\boldsymbol{k}_\perp)\Phi_A(y_q,\boldsymbol{q}_\perp+\boldsymbol{k}_\perp) + \Phi_B^2(y_q,\boldsymbol{k}_\perp)\Phi_A(y_p,\boldsymbol{p}_\perp-\boldsymbol{k}_\perp)\Phi_A(y_q,\boldsymbol{q}_\perp-\boldsymbol{k}_\perp). \quad (9)$$

Since uGD (Φ) peaks at Q_s, transverse momentum far from Q_s contributes little to the correlation. To make a significant contribution to the correlation function,

$$|\boldsymbol{k}_\perp| \sim Q_s, |\boldsymbol{p}_\perp-\boldsymbol{k}_\perp| \sim Q_s \quad \text{and} \quad |\boldsymbol{q}_\perp-\boldsymbol{k}_\perp| \sim Q_s \quad (10)$$

are required simultaneously in the second terms of both D_1 and D_2. If $\boldsymbol{p}_\perp$ and $\boldsymbol{q}_\perp$ are identical, and consequently $\boldsymbol{p}_\perp-\boldsymbol{k}_\perp = \boldsymbol{q}_\perp-\boldsymbol{k}_\perp$, the above conditions can be satisfied simultaneously, which leads to collimation production at $\Delta\phi = 0$. Similarly, significant contributions from the first terms of D_1 and D_2 require $\boldsymbol{p}_\perp$ and $\boldsymbol{q}_\perp$ are antiparallel, which leads to collimation production at $\Delta\phi = \pi$. This explains why two gluons that are collimated have the strongest correlations.

On the other hand, uGD only depends on the magnitude of transverse momentum, not on its direction. In that case, we should only require an equal module of the two arguments, i.e., $|\boldsymbol{p}_\perp-\boldsymbol{k}_\perp| \sim |\boldsymbol{q}_\perp-\boldsymbol{k}_\perp| \sim Q_s$. Two parallel or antiparallel transverse momenta are sufficient but unnecessary conditions for large correlations. According to the triangle law of vector addition, $\boldsymbol{k}_\perp$, $\boldsymbol{p}_\perp$, and $\boldsymbol{p}_\perp-\boldsymbol{k}_\perp$ constitute the three edges of a triangle. Since the maximum of uGD needs $|\boldsymbol{k}_\perp| \sim Q_s$ and $|\boldsymbol{p}_\perp-\boldsymbol{k}_\perp| \sim Q_s$, the angle between $\boldsymbol{k}_\perp$ and $\boldsymbol{p}_\perp$ [denoted as $\Delta\phi_{kp}$, which satisfies $\cos(\Delta\phi_{kp}) = \frac{|\boldsymbol{k}_\perp|^2+|\boldsymbol{p}_\perp|^2-|\boldsymbol{p}_\perp-\boldsymbol{k}_\perp|^2}{2|\boldsymbol{k}_\perp||\boldsymbol{p}_\perp|}$] is determined by $|\boldsymbol{p}_\perp|$. So is $\Delta\phi_{kq}$. Thus, the relative azimuth $\Delta\phi = \phi_q - \phi_p$ at which correlations become significant depends on the magnitude of the two momenta. That explains why the peak position between $\Delta\phi = 0$ and π varies with transverse momenta, as shown in Figs. 3(a) and 3(b). Since Q_s is y dependent, two edges in that triangle depend on y. For given $p_\perp$, $\Delta\phi_{kp}$ varies with y, which means the relative azimuth at which correlations become significant depends on rapidity y. At some momenta or rapidity, the correlations show a simple structure of a valley between $\Delta\phi = 0$ and π, without bumps and shoulders. That is because the lengths of the three edges are not appropriate to form a triangle and hence the uGDs cannot get a maximum simultaneously to develop a large correlation.

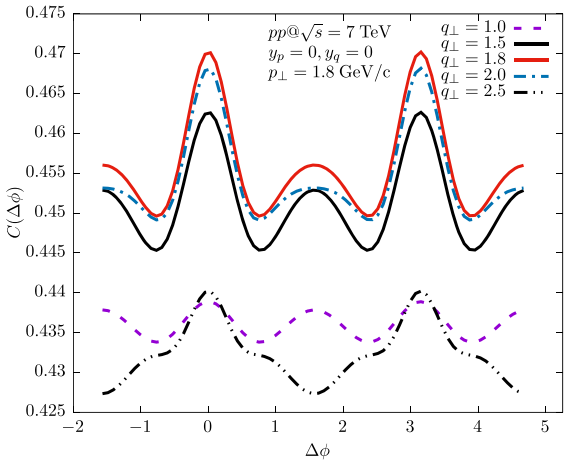

FIG. 4. Azimuthal correlations at five values of $q_\perp$ with $p_\perp = 1.8$ GeV/c at $y_p = 0$, $y_q = 0$.

From this point of view, we can infer that if $p_\perp$ is fixed the azimuthal correlation pattern for different $q_\perp$ should be different. This is indeed the case, as shown in Fig. 4. To observe the fine correlation patterns, $p_\perp$ is chosen as 1.8 GeV/c, and $y_p = 0$, $y_q = 0$ with both gluons at small rapidity. When $q_\perp$ varies from 1.0 to 2.0 GeV/c, the peak at $\Delta\phi = \pi/2$ always exists, despite differences of its strength. When $q_\perp$ departs from the sensitive range, the peak reduces to double shoulders. This indicates that these correlation patterns require that at least one gluon has transverse momentum within the sensitive range.

IV. SUMMARY AND DISCUSSION

In this paper, we study two-gluon azimuthal correlations and their $p_\perp$ and y dependence by using the CGC formalism. We find that two-gluon azimuthal correlations are sensitive to the detailed dynamical features of the CGC. Here, two gluons are both chosen from small rapidity location or both chosen from the large rapidity location, or one is chosen from the small rapidity location and the other is chosen from large rapidity location. Results show that azimuthal correlations at the same rapidity gap change with the rapidity location of the chosen gluon. Fine structures around $\Delta\phi = \pi/2$, i.e., bumps or shoulders, show up when at least one gluon is located at small rapidity, which suggests that fine structures of correlation patterns are specific to the small-x region. A single value of $p_\perp$ near $Q_{sA} + Q_{sB} = 2Q_{sp} = 1.8$ GeV/c, instead of integration over $p_\perp$ in a wide range like $1 < p_\perp < 2$ GeV/c, is more likely to illustrate fine structures between $\Delta\phi = 0$ and π. The fine structures around $\Delta\phi = \pi/2$ correspond to high-order harmonic components in a Fourier expansion. That means high-order harmonic components only get prominent when at least one gluon is located at small rapidity and at least one gluon has transverse momentum near $2Q_{sp}$ (the sum of the saturation momentum of two colliding particles).

As we addressed in the Introduction, the mechanisms of gluon production at different rapidity locations are different. So, the study on the effect of the rapidity location, other than the rapidity range, on azimuthal correlations, helps to reveal the fine structures in azimuthal correlations, which are absent in the pioneer papers [13–17].

As pointed out in our previous paper [22], the correlations between both radiated gluons are smaller than those between both source gluons. The ridge correlations are more relevant to source gluons at large rapidity. The phenomenon at small rapidity in this manuscript is induced by radiated gluons. Since correlations between radiated gluons that are located at the small rapidity location are relatively weak, the fine structures are easier to see at the small rapidity location.

Furthermore, the shape of azimuthal correlations is also sensitive to the transverse momentum. The sensitivity of the azimuthal correlation structures to the transverse momentum in our calculations stems from an intrinsic scale (the saturation momentum) in which the initial-state wave function peaks. Fine structures likely appear at the transverse momentum close to the sum of saturation scales of the projectile and target. As our calculations illustrate, fine structures are more obvious in the case of a single value of $p_\perp$ and are nearly smeared by an integration over $p_\perp$ in a width of 1 GeV/c. So, a narrow bin of $p_\perp$, much less than 1 GeV/c, will help to see the fine structure; otherwise, the bumps will be less noticeable.

The fine structures in azimuthal correlations are associated with small x and saturation momentum, and hence they may provide the possibility of testing glasma dynamics in experiment. However, since these correlations occur at very early times, a proper understanding of the later-stage interactions is required.

As we know, flow contributes to azimuthal correlations. It would increase the height of the azimuthal correlations. It would not change the fine structures significantly in p-p collisions.

Moreover, another final-state factor that should be considered is fragmentation functions. In Ref. [34], soft and hard fragmentation functions are used, and results show that fragmentation functions have a major impact on transverse momentum dependence. Since including fragmentation functions brings integrations over z, the transverse momentum fraction of the produced hadron with respect to that of the fragmenting gluon, the azimuthal correlations of two hadrons at a certain transverse momentum, e.g., p_0, take into account the contributions of all gluons with transverse momenta larger than p_0. The wide integration interval over $p_\perp$ of gluons will smear the fine structures found at the gluon level. Another hadronization mechanism frequently used in Mont Carlo simulations, called the coalescence model, may also smear the fine structures in azimuthal correlations due to a wide variety of combinations of gluon transverse momentum into a hadron with certain transverse momentum.

However, if parton-hadron duality holds [16], the signal in the azimuthal patterns would remain in the final state. Therefore, it is still interesting to check carefully in high-energy p-p collisions if this fine structure exists in the final state.

ACKNOWLEDGMENTS

This work is supported in part by the Major State Basic Research Development Program of China under Grant No. 2014CB845402, the Ministry of Science and Technology of the People's Republic of China under Grant No. 2016YFE0104800, the National Natural Science Foundation of China under Grants No. U1732271 and No. 11647093, and the China Scholarship Council under Grant No. 201706775081.

[1] A. Adare *et al.* (PHENIX Collaboration), Phys. Rev. C **78**, 014901 (2008).
[2] B. Alver *et al.* (PHOBOS Collaboration), Phys. Rev. Lett. **104**, 062301 (2010).
[3] CMS Collaboration, J. High Energy Phys. 09 (2010) 091.
[4] J. Adams *et al.* (STAR Collaboration), Phys. Rev. Lett. **95**, 152301 (2005).
[5] B. I. Abelev *et al.* (STAR Collaboration), Phys. Rev. C **80**, 064912 (2009).
[6] CMS Collaboration, Phys. Lett. B **724**, 213 (2013).
[7] CMS Collaboration, Phys. Lett. B **718**, 795 (2013).
[8] ATLAS Collaboration, Phys. Rev. Lett. **110**, 182302 (2013).
[9] ALICE Collaboration, Phys. Lett. B **719**, 29 (2013).
[10] ALICE Collaboration, Phys. Lett. B **753**, 126 (2016).
[11] A. Adare *et al.* (PHENIX Collaboration), Phys. Rev. Lett. **114**, 192301 (2015).
[12] A. Adare *et al.* (PHENIX Collaboration), Phys. Rev. Lett. **115**, 142301 (2015).
[13] A. Dumitru, F. Gelis, L. McLerran, and R. Venugopalan, Nucl. Phys. **A810**, 91 (2008).
[14] K. Dusling, F. Gelis, T. Lappi, and R. Venugopalan, Nucl. Phys. **A836**, 159 (2010).
[15] K. Dusling and R. Venugopalan, Phys. Rev. D **87**, 051502 (R) (2013).
[16] K. Dusling and R. Venugopalan, Phys. Rev. D **87**, 054014 (2013).
[17] K. Dusling and R. Venugopalan, Phys. Rev. D **87**, 094034 (2013).

[18] A. Bzdak and G.-L. Ma, Phys. Rev. Lett. **113**, 252301 (2014).
[19] See a review: K. Dusling, W. Li, and B. Schenke, Int. J. Mod. Phys. E **25**, 1630002 (2016).
[20] K. Werner, I. Karpenko, and T. Pierog, Phys. Rev. Lett. **106**, 122004 (2011); P. Bozek and W. Broniowski, Phys. Lett. B **718**, 1557 (2013); G. Y. Qin and B. Muller, Phys. Rev. C **89**, 044902 (2014).
[21] B. Abelev *et al.* (ALICE Collaboration), Phys. Lett. B **719**, 29 (2013).
[22] Y.-Y. Zhao, M.-M. Xu, H.-Y. Zhang, and Y.-F. Wu, Nucl. Phys. **A955**, 88 (2016).
[23] L. V. Gribov, E. M. Levin, and M. G. Ryskin, Phys. Rep. **100**, 1 (1983).
[24] E. Iancu and R. Venugopalan, arXiv:hep-ph/0303204.
[25] H. Weigert, Prog. Part. Nucl. Phys. **55**, 461 (2005).
[26] F. Gelis, E. Iancu, J. Jalilian-Marian, and R. Venugopalan, Annu. Rev. Nucl. Part. Sci. **60**, 463 (2010).
[27] J. Jalilian-Marian, A. Kovner, L. D. McLerran, and H. Weigert, Phys. Rev. D **55**, 5414 (1997).
[28] J. Jalilian-Marian, A. Kovner, A. Leonidov, and H. Weigert, Phys. Rev. D **59**, 014014 (1998).
[29] E. Iancu, A. Leonidov, and L. D. McLerran, Phys. Lett. B **510**, 133 (2001).
[30] I. Balitsky, Nucl. Phys. **B463**, 99 (1996).
[31] I. Balitsky, Phys. Rev. D **60**, 014020 (1999).
[32] Y. V. Kovchegov, Phys. Rev. D **60**, 034008 (1999).
[33] Y.-Y. Zhao, M.-M. Xu, H.-Y. Zhang, and Y.-F. Wu, arXiv:1709.08678.
[34] K. Dusling and R. Venugopalan, Phys. Rev. Lett. **108**, 262001 (2012).